

Nurbatyr Mukhametgazy¹, Kamila M. Temirkulova^{1,2}, Balausa Balgabayeva^{1,2},
Bekzat G. Khamzin^{1,2}, Seitkhan Azat¹, Zhazira A. Supiyeva^{1,2*}, Qamar Abbas^{3,4}

¹Satbayev University, Almaty, Kazakhstan;

²Al-Farabi Kazakh National University, Almaty, Kazakhstan;

³Graz University of Technology, Graz, Austria;

⁴Poznan University of Technology, Poznan, Poland

(*Corresponding author's e-mail: zhazira.supiyeva@kaznu.kz)

Effect of Activating Agent and Temperature Conditions on the Electrochemical Performance of Rice Husk-Based Activated Carbon in Supercapacitors

This study investigates the electrochemical properties of activated carbon (AC) derived from rice husk, focusing on the influence of activation conditions using NaOH and KOH at temperatures of 650 °C, 750 °C, and 850 °C. The results demonstrate that RH-AC/KOH activated at 750 °C exhibits the highest capacitance retention (159–165 F·g⁻¹) and superior electrochemical performance, attributed to its optimized microporous structure and enhanced electrical conductivity. These properties make it an excellent candidate for electrode material in supercapacitors. Electrochemical evaluations, including cyclic voltammetry (CV), galvanostatic charge-discharge (GCD), and electrochemical impedance spectroscopy (EIS), confirm that RH-AC/KOH activated at 750 °C delivers the highest current density, stable performance across a wide voltage range (0.6–1.5 V), and the longest discharge duration. A comparison of the specific current change (ΔSc) at low potentials (0.6–1.0 V) for the four samples AC/NaOH at 850 °C and RH-AC/KOH at 750 °C, 650 °C, and 850 °C shows the following trend: 281.2 > 269.2 > 267.6 > 190.5 mA·g⁻¹. At higher potentials (1.2–1.5 V), the ΔSc values follow the order: 341.9 ≈ 340.0 > 314.6 > 247.8 mA·g⁻¹. These findings identify RH-AC/KOH activated at 750 °C as a highly promising electrode material for next-generation supercapacitors, offering unique energy storage capacity, stability, and long-term durability.

Keywords: activated carbon, rice husk, chemical activation, thermal post-treatment, electrical properties, electrical conductivity, supercapacitors, electrode material, energy storage

Introduction

Activated carbon (AC) is widely used in energy storage applications, particularly in supercapacitors and batteries, due to its high surface area, good electrical conductivity, and relatively low cost [1, 2]. AC can be prepared through several methods, including physical activation (using gases such as CO₂, H₂, or CH₄) and chemical activation (using agents like ZnCl₂, NaOH, KOH, or H₃PO₄). Chemical activation typically involves thermal treatment of a carbon precursor with an activating agent at temperatures ranging from 450 to 900 °C. This method offers distinct benefits compared to physical activation [3]. The resulting porous structure, which includes micro-, meso-, and macropores, makes activated carbon a suitable material for a wide range of industrial and environmental applications [4]. Numerous studies have investigated the influence of processing conditions on the physicochemical properties of AC derived from biowaste sources such as rice husk and walnut shells. Some of these studies have even developed predictive models for estimating AC performance characteristics [5–8]. Nevertheless, there remains significant potential to optimize biowaste-derived AC synthesis methods and explore new applications. Recently, increasing attention has been given to the use of such materials in supercapacitors and hydrogen storage systems. Depending on the energy storage mechanism, supercapacitors (SCs) utilizing AC can be categorized into three main types: electric double-layer capacitors (EDLCs), pseudocapacitors, and hybrid supercapacitors, which combine features of the first two [9]. As research progresses, supercapacitor technology is considered one of the most promising and efficient solutions for next-generation energy storage devices [10, 11].

Despite their advantages, ACs also have certain limitations, including increased internal resistance and reduced power output in energy storage devices [12–14]. Moreover, producing high-quality ACs often requires high-temperature pyrolysis and strong chemical activating agents, such as acids or bases, which can have harmful environmental effects [15, 16]. However, the rapid charging and discharging capacity of super-

capacitors gives them a significant advantage over traditional batteries. From this perspective, one of the key challenges lies in supporting high-speed electric motors, such as those used in electric vehicle engines and specialized equipment. Consequently, biowaste-derived ACs have attracted strong interest from scientists and companies as a promising electrode material for supercapacitor production. In recent years, numerous agricultural by-products have been investigated as sustainable precursors for ACs production, including coconut shells, corn cobs, lignocellulosic biomass, walnut shells, and peanut shells [17–20]. These biomass sources are typically rich in carbon and exhibit a high potential for porosity development, both of which are critical for electrochemical energy storage applications. While abundantly available, walnut shells and corn cobs tend to produce ACs with irregular pore size distributions and limited mesoporosity, restricting ion transport in supercapacitor systems [21, 22]. In contrast, rice husk (RH) is particularly advantageous due to its intrinsic high silica content, which acts as a natural template promoting hierarchical pore formation during activation [23]. Furthermore, RH-derived ACs have consistently demonstrated higher surface areas, better electrical conductivity, and enhanced electrochemical performance compared to other biomass-derived carbons [24]. Importantly, Kazakhstan produces a substantial amount of RH as agricultural waste, especially in rice-producing regions, making it a readily available and cost-effective resource for value-added conversion into energy storage materials [25].

In addition to carbonization temperature and the type of chemical activating agent, several other experimental parameters play an important role in tailoring the structural and electrochemical properties of ACs [26, 27]. Factors, namely activation time, heating rate, precursor particle size, and the atmosphere during carbonization significantly influence porosity, specific surface area, and conductivity, key characteristics that determine ACs performance in applications such as supercapacitors. For instance, prolonged activation time can promote pore development but may also lead to pore collapse if overextended [28]. Similarly, slower heating rates favor more uniform pore structures and higher surface areas [29], while smaller precursor particles have been associated with enhanced textural properties and ion accessibility [30]. Moreover, the carbonization atmosphere (such as nitrogen gas, steam, or CO₂) affects both the physical and chemical properties of the carbon surface, with steam activation often introducing functional groups that improve wettability and electrochemical performance [31, 32]. Therefore, the synergistic optimization of all these conditions is essential to maximize the performance of biomass-derived ACs [33]. This is assessed through rate capability tests (ranging from 0.1 to 10 A·g⁻¹) and long-term stability tests, including voltage floating (100 hours at a cell voltage of 2.7 V) [34]. In our previous studies [35, 36], we compared various thermal treatment methods for synthesizing activated carbon from walnut shells, with the goal of optimizing production processes [5, 7]. To achieve the best electrochemical performance from electrodes, fine-tuning and optimization, especially for activated carbon-based electrodes, are essential. In this study, two activation agents, NaOH and KOH, were used to produce activated carbons at a temperature of 850 °C. After conducting a comparative analysis, it was found that KOH was the more effective agent. As a result, additional tests at 650 °C and 750 °C were performed, and the resulting carbons were evaluated as electrodes in supercapacitors. Ultimately, the comparative analysis revealed that AC activated with KOH at 750 °C delivered the best electrochemical performance among all tested samples.

This study presents a comprehensive investigation into the optimization of rice husk-derived activated carbon for use in supercapacitor electrodes, with a particular focus on the effects of activation temperature (650, 750, and 850 °C) and chemical activating agents (NaOH and KOH). The electrochemical performance of the synthesized carbons was systematically compared across the tested temperatures. The findings provide valuable insights into the optimal activation conditions, demonstrating that activation with KOH at 750 °C yields the most favorable results for enhancing supercapacitor efficiency. Future work will involve cycling stability and capacitance retention testing under extended voltage ranges (beyond 1.5 V), with the goal of further improving the long-term performance and reliability of supercapacitor devices.

Experimental

Materials

Rice husk (RH) was sourced from the Kyzylorda Region, Kazakhstan. The activation agents, sodium hydroxide (NaOH), potassium hydroxide (KOH) with 98 % purity, Carbon black (C₆₅, Timcal C-ENERGY Imerys), and polytetrafluoroethylene (PTFE, 60 % dispersion in water) were purchased from Sigma-Aldrich Chemical Co. (USA) and used without further purification. Nitrogen gas (99.95 wt.% purity, “Ikhsan TechnoGas” Ltd., Almaty, Kazakhstan) was used for the second carbonization step at 500 °C with a heating rate of 7.5–8 °C·min⁻¹. Gas activation was carried out under N₂ atmosphere at a flow rate of 150 mL·min⁻¹. Dis-

tilled water (resistivity $\approx 1\text{--}10\text{ M}\Omega\cdot\text{cm}$) and deionized water (DI, resistivity $\geq 18.2\text{ M}\Omega\cdot\text{cm}$) were prepared in-house and used for washing and synthesis procedures. Ethanol was purchased from “Laborfarma” LLP, Almaty, Kazakhstan.

Methods

Synthesis of RH-Based Activated Carbon

Activated carbon was synthesized from rice husk using NaOH and KOH as activating agents under various high-temperature treatment conditions. Initially, the rice husk was thoroughly washed multiple times with distilled water to remove dirt and surface impurities. After cleaning, it was dried to a constant mass and subjected to preliminary carbonization at $500\text{ }^\circ\text{C}$ ($\pm 10\text{ }^\circ\text{C}$) for 1 hour under a nitrogen atmosphere to prevent oxidation [11, 12]. Chemical activation was carried out at $850\text{ }^\circ\text{C}$ ($\pm 10\text{ }^\circ\text{C}$) for 1 hour under nitrogen flow. For post-thermochemical activation, the carbonized rice husk was mixed with KOH powder and thermally treated in air at $650\text{ }^\circ\text{C}$, $750\text{ }^\circ\text{C}$, and $850\text{ }^\circ\text{C}$ for 5 hours to ensure full impregnation of the carbon structure by molten KOH. Both sodium hydroxide (NaOH) and potassium hydroxide (KOH) were used as activating agents, with a precursor-to-activating agent mass ratio of 1:4. After activation, the resulting samples were washed with hot distilled water until a neutral pH (6-7) was achieved, ensuring the removal of residual alkali. The materials were then dried at $100\text{ }^\circ\text{C}$ for 24 hours. The dried activated carbon was ground and subjected to a second carbonization step at $500\text{ }^\circ\text{C}$ for 90 minutes under an argon atmosphere, with a heating rate of $7.5\text{--}8\text{ }^\circ\text{C}\cdot\text{min}^{-1}$, following the procedure described previously [5, 36]. The resulting RH-AC samples prepared by this method were used in the fabrication of a supercapacitor cell, as described in the next section.

Electrode Fabrication and Electrochemical Tests

A symmetrical two-electrode system was employed, in which both the working and counter electrodes were fabricated from the same activated carbon material derived from rice husk. Additionally, the supercapacitor cell was equipped with an Ag/AgCl reference electrode and a stainless steel current collector. To prepare the activated carbon electrodes (Carbon/C₆₅/PTFE), a composite mixture was formulated consisting of 90 wt.% activated carbon powder, 5 wt.% carbon black (C65) as a conductive additive, and 5 wt.% polytetrafluoroethylene (PTFE, 60 % dispersion in water), resulting in a 90:5:5 weight ratio. The components were thoroughly mixed and ground using an agate mortar and pestle until the solvent fully evaporated. The resulting mixture was dried overnight in a vacuum oven at $120\text{ }^\circ\text{C}$. Afterwards, disc-shaped electrodes (10 mm diameter) were punched from the formed sheet, yielding a final thickness of approximately $100\text{ }\mu\text{m}$ [37].

Table 1

Rice husk-based activated carbon (RH-AC) electrodes

AC	Mass values of AC combinations		
	Carbon, g	C ₆₅ , g	PTFE, g
NaOH — $850\text{ }^\circ\text{C}$	0.2547	0.0151	0.0141
RH — $650\text{ }^\circ\text{C}$	0.2893	0.0163	0.0162
RH — $750\text{ }^\circ\text{C}$	0.2793	0.0155	0.01506
RH — $850\text{ }^\circ\text{C}$	0.2909	0.0161	0.0165

The electrochemical performance of RH-AC in a supercapacitor was evaluated using cyclic voltammetry (CV), galvanostatic charge-discharge (GCD) measurements, and electrochemical impedance spectroscopy (EIS). The CV measurements were carried out within a voltage range of $0.6\text{--}1.5\text{ V}$ at various scan rates. GCD tests were conducted at a constant current of $0.2\text{ A}\cdot\text{g}^{-1}$ to determine specific capacitance and energy density at different current densities, with a potential cutoff of 2 mV . EIS analysis was performed using a VMP-3 multichannel potentiostat/galvanostat (BioLogic Instruments, France) over a frequency range of 100 mHz to 100 kHz to investigate charge transfer resistance and ion diffusion properties [37]. Electrochemical studies were carried out using VSP-300 electrochemical workstations. The CV curves were recorded within a 1 V potential window, while GCD tests were performed at a constant current of $0.2\text{ A}\cdot\text{g}^{-1}$. Impedance measurements were conducted in the $100\text{ kHz}\text{--}10\text{ mHz}$ frequency range with a potential amplitude of 1.5 V . The specific capacitance was calculated from GCD curves using the following equation:

$$C = \frac{4I\Delta t}{m\Delta V}, \quad (1)$$

where C ($\text{F}\cdot\text{g}^{-1}$) is the specific capacitance; I (A) is the discharge current; Δt (s) is the discharge time; ΔV (V) is the potential window; m (mg) is the total mass of two electrodes.

Specific capacitance from the CV curve was calculated using the following equation:

$$C = \frac{2}{mv(V_b - V_a)} \int_{V_a}^{V_b} IdV. \quad (2)$$

Here, C ($\text{F}\cdot\text{g}^{-1}$) represents the specific capacitance, m (mg) denotes the total mass of both electrodes, v ($\text{mV}\cdot\text{s}^{-1}$) is the scan rate, I (A) refer to the discharge current, and V_b and V_a correspond to the upper and lower voltage limits in the cyclic voltammetry (CV) test [38].

Result and Discussion

Characterization of RH-based AC in a Supercapacitor System

The microstructural characteristics of carbon materials derived from rice husks after thermochemical activation were extensively examined in our previous study [35]. The SEM micrographs of RH-AC revealed a well-developed porous architecture within the carbon matrix, formed through carbonization and graphitization at 750°C , followed by KOH-assisted thermochemical activation at 850°C . The resulting material exhibited a uniform distribution of macropores across the surface. The specific surface area of the rice husk-derived activated carbon reached $2290\text{ m}^2\cdot\text{g}^{-1}$, enhancing its suitability for electrochemical applications [36]. Building upon these prior findings, the present study investigates the electrochemical performance of RH-based activated carbons (RH-ACs) in a supercapacitor system, with a particular focus on specific capacitance behavior across a voltage range of $0.6\text{--}1.5\text{ V}$ at varying scan rates. The influence of activation parameters, particularly the choice of chemical activator (KOH vs. NaOH) and activation temperatures (650°C , 750°C , and 850°C), is evaluated using CV, GCD, and EIS to determine the optimal RH-AC materials for use as suitable cathodes in supercapacitors.

Figure 1 presents CV results of two electrodes (2E) in SC systems fabricated using four activated carbon samples: AC/NaOH at 850°C (black), RH-AC/KOH at 650°C (red), RH-AC/KOH at 750°C (blue), and RH-AC/KOH at 850°C (green). Specific capacitance was evaluated across voltage ranges from 0.6 to 1.5 V to assess charge storage efficiency and ion transport properties.

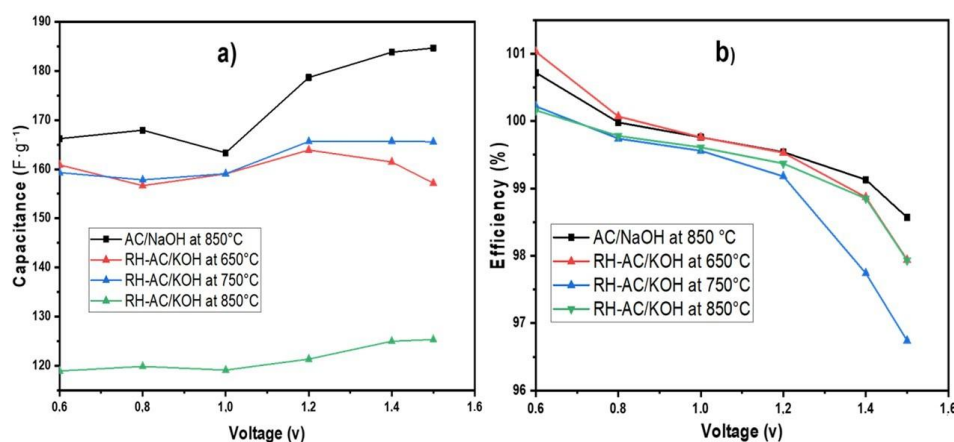


Figure 1. CV results showing (a) specific capacitance and (b) coulombic efficiency of 2E-type electrodes based on AC/NaOH and RH-AC/KOH samples activated at different temperatures, measured across a voltage range of $0.6\text{--}1.5\text{ V}$ at a scan rate of 2 mV/s

Figure 1(a) shows that AC/NaOH sample activated at 850°C exhibited a stable and gradually increasing capacitance, ranging from 166 to $184\text{ F}\cdot\text{g}^{-1}$, except for a slight dip at 1.0 V ($163\text{ F}\cdot\text{g}^{-1}$), suggesting a well-developed pore structure. In contrast, RH-AC/KOH activated at 650°C displayed a sharp decrease in capacitance from 161 to $157\text{ F}\cdot\text{g}^{-1}$, likely due to insufficient activation and poor electrical conductivity. RH-AC/KOH at 850°C showed the lowest capacitance (119 to $125\text{ F}\cdot\text{g}^{-1}$), attributed to excessive pore widening and reduced availability of effective charge storage sites. The RH-AC/KOH at 750°C demonstrated the best capacitance retention (159 to $165\text{ F}\cdot\text{g}^{-1}$), based on the microporosity and conductivity, making it the most effective cathode material for supercapacitor applications. Figure 1(b) illustrates the coulombic efficiency of

four different AC samples in a supercapacitor system. The performance of each sample is analyzed based on capacitance retention as a function of voltage variation within the range of 0.6 to 1.5 V. The efficiency of each sample was evaluated across the voltage range, showing a gradual decline. At the initial voltage of 0.6 V, the efficiencies of AC/NaOH at 850 °C and RH-AC/KOH at 650 °C, 750 °C, and 850 °C were all close to 100 %. By the final voltage of 1.5 V, the efficiency values were approximately 98.6 %, 100 %, 96.7 %, and 100 %, respectively. The RH-AC/KOH at 750 °C displayed slightly lower efficiency compared to the other samples at 1.5 voltage.

The CV curves of two electrode (2E) cells with AC/NaOH at 850 °C and RH-AC/KOH at 650 °C, 750 °C, and 850 °C, measured up to 1.0 V in 1 mol·L⁻¹ Li₂SO₄ electrolyte, are shown in Figure 2 (a, b, c, and d), respectively. As shown in Figure 2(a), the CV curves of AC/NaOH at 850 °C exhibit capacitance traces with a specific current (*Sc*) ranging from -135.6 to 145.6 mA·g⁻¹ in the lower potential region (0.6–1.0 V), while in the higher potential region (1.2–1.5 V), the specific current varies from -157 to 184.9 mA·g⁻¹. The specific current change (ΔSc) at low and high voltages was calculated as 281.2 and 341.9 mA·g⁻¹, respectively. Figure 2(b) presents the CV curves of RH-AC/KOH at 650 °C, showing capacitance traces where the specific current increases from -143.9 to 123.7 mA·g⁻¹ in the low potential region. At higher potentials, the specific current varies from -157 to 184.9 mA·g⁻¹. The corresponding ΔSc values for low and high potentials were determined to be 267.6 and 314.6 mA·g⁻¹, respectively. Similarly, as shown in Figure 2(c), the CV curves of RH-AC/KOH at 750 °C exhibit specific current variations from -135.7 to 133.5 mA·g⁻¹ in the low potential region and from -155.6 to 184.4 mA·g⁻¹ in the higher potential region. The ΔSc values for these voltage ranges were calculated as 269.2 and 340.0 mA·g⁻¹, respectively. In Figure 2(d), the cyclic voltammetry (CV) curves for the RH-AC/KOH sample at 850 °C show that the specific current ranges from -88.4 to 190.5 mA·g⁻¹ at lower potentials and from -106.4 to 141.4 mA·g⁻¹ at higher potentials.

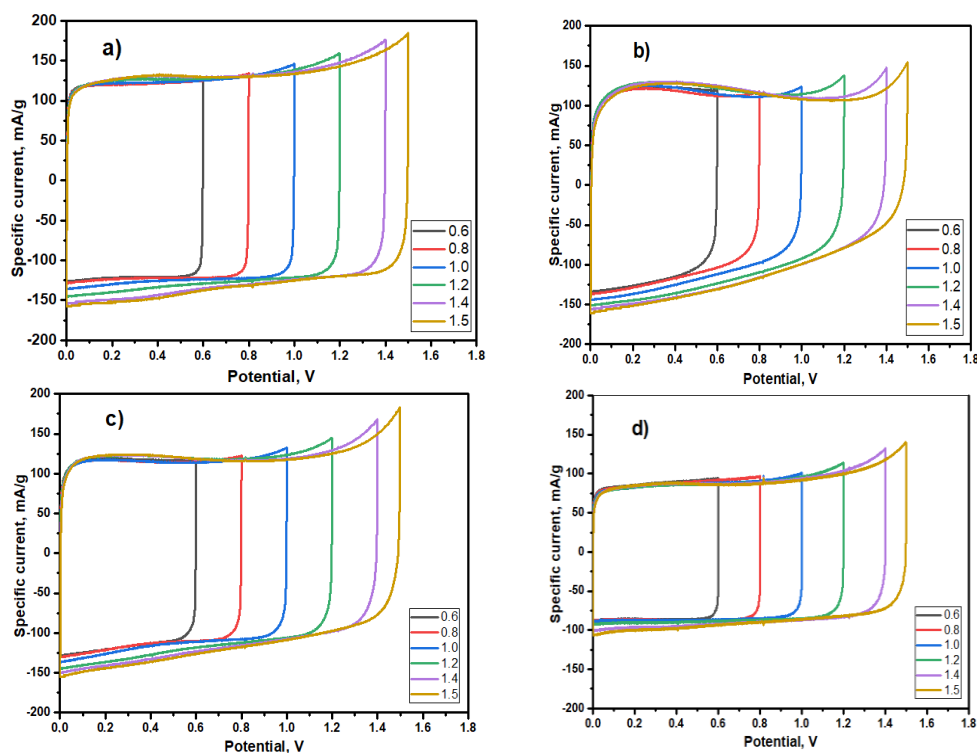


Figure 2. CV curves at 2 mV/s of 2E cell with AC/NaOH at 850 °C (a) and RH-AC/KOH at 650 (b), 750 (c) 850 °C (d) activated electrodes in different voltages

The corresponding changes in specific current (ΔSc) are 190.5 mA·g⁻¹ and 247.8 mA·g⁻¹, respectively. A comparison of ΔSc values at low voltages among the four samples, namely AC/NaOH at 850 °C and RH-AC/KOH at 750 °C, 650 °C, and 850 °C reveals the following trend: 281.2 > 269.2 > 267.6 > 190.5 mA·g⁻¹. Similarly, in the high voltage range, the ΔSc values follow the order: 341.9 \approx 340.0 > 314.6 > 247.8 mA·g⁻¹. From these results, it is evident that the electrode density of AC/NaOH at 850 °C is significantly higher. Among the RH-AC/KOH samples, the one treated at 750 °C exhibits the highest current

density, comparable to that of AC/NaOH at 850 °C. These electrochemical results indicate that RH-AC/KOH at 750 °C achieves the highest current density, signifying superior electrochemical performance.

Figure 3 shows the galvanostatic charge-discharge (*a*), and electrochemical impedance (*b*) of AC/NaOH 2E cell at a current density of $0.2 \text{ A}\cdot\text{g}^{-1}$ in different voltage ranges at 850 °C. Figure 3 (*a*) shows a triangular shape within the voltage range of 0.6–1.5 V, which suggests nearly ideal capacitive behavior, as is typical of double-layer capacitors. The initial voltage drop during discharge, which occurs between 259 and 531 seconds, appears minimal. A total discharge duration of 272 seconds indicates low internal resistance and excellent conductivity of the electrode materials. The longest discharge time is observed at 1.5 V, with a maximum discharge time of 671 seconds exhibiting the highest stored charge value between 671 and 1342 seconds. At higher voltages (1.4 V and 1.5 V), the charge-discharge curves remain linear with a right angle, indicating good electrode stability even under elevated voltage conditions. Additionally, the charge-discharge curves are symmetrical and consist of straight lines, showing consistent growth as the voltage increases from 0.6 to 1.5 V. Figure 3(*b*) demonstrates the Nyquist Plot (EIS) at different voltages (0.6–1.5 V). The shift in charge transfer resistance (R_{ct}) at lower voltages 0.6–1.0 shows the same $0.6 \text{ }\Omega$ and low Equivalent Series Resistance (R_s) $0.27 \text{ }\Omega$. The small semicircle at high frequencies corresponds to the charge transfer resistance (R_{ct}) at the electrode/electrolyte interface [36]. According to the specified parameters, the R_{ct} values for the three voltages in 1.2 V, 1.4 V, and 1.5 V gradually increase to $0.73 \text{ }\Omega$, $1.21 \text{ }\Omega$, and $2.05 \text{ }\Omega$, respectively. Correspondingly, the R_s values are $0.32 \text{ }\Omega$, $0.41 \text{ }\Omega$, and $0.56 \text{ }\Omega$, respectively. A larger semicircle at higher voltages (1.4 V and 1.5 V) is attributed to an increase in R_{ct} . The highest change in charge transfer resistance (ΔR_{ct}) is $1.49 \text{ }\Omega$, which is possibly due to reduced ionic conductivity at higher voltages compared to lower voltage ranges. The ECI measurement results (Fig. *b*) suggest that the enhanced R_{ct} values of AC/NaOH 2E cells reflect a notable alteration in the porous structure that facilitates easier electrolyte diffusion.

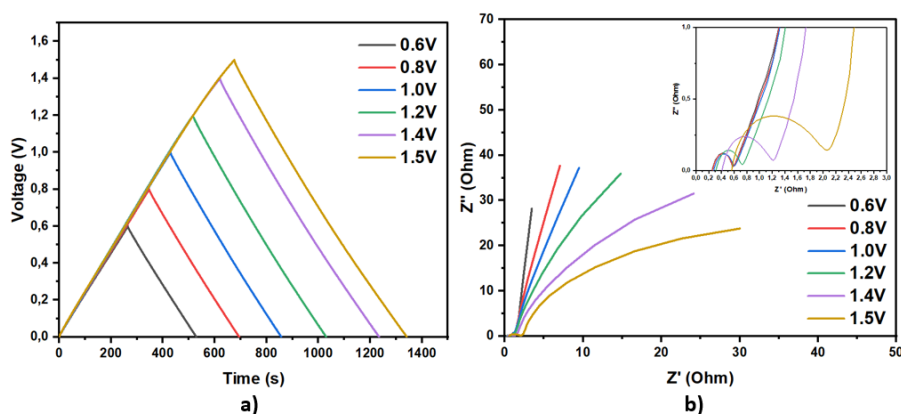


Figure 3. GCD (*a*) and EIS (*b*) curves of the AC/NaOH 2E cell at a current density of $0.2 \text{ A}\cdot\text{g}^{-1}$ in different voltage ranges at 850 °C

Figure 4 shows the charge-discharge behavior and electrochemical impedance of a 2E cell with RH-AC treated with KOH at 650 °C, 750 °C, and 850 °C at a current density of $0.2 \text{ A}\cdot\text{g}^{-1}$, across various voltage limits. Figure 4(*a*) shows that the initial voltage drop during discharge, occurring between 248 and 498 seconds, is minimal. Moreover, the total discharge duration (ΔT) of 250 seconds suggests low internal resistance and excellent conductivity of the electrode materials. The longest discharge time is notably observed at 1.5 V, ranging from 563 to 1124 seconds, with a maximum duration of (ΔT) 561 seconds, indicating the highest stored charge value. However, the GCD properties of RH-AC/KOH at 650 °C are significantly lower than those of AC/NaOH 2E at 850 °C. Furthermore, at higher voltages (1.4 V and 1.5 V), the charge-discharge curves deviate from linearity; a curved line reduces symmetry rather than a right angle. In contrast, its stability declines as the voltage increases from 1.2 to 1.5 V. Figure 4(*d*) presents the Nyquist plot of RH-AC/KOH at 650 °C. At low voltages (0.6–1.0 V), the charge transfer resistance (R_{ct}) and equivalent series resistance (R_s) remain similar, with values of $2.86 \text{ }\Omega$ and $0.47 \text{ }\Omega$, respectively. As the voltage increases to 1.2 V, 1.4 V, and 1.5 V, the R_{ct} values rise uniformly to $3.5 \text{ }\Omega$, $5.2 \text{ }\Omega$, and $7.16 \text{ }\Omega$, respectively. Similarly, the R_s values increase to $0.56 \text{ }\Omega$, $0.72 \text{ }\Omega$, and $0.84 \text{ }\Omega$. The most significant increase in charge transfer resistance is observed at the highest voltage (1.5 V), reaching $7.16 \text{ }\Omega$ due to the formation of a large semicircle.

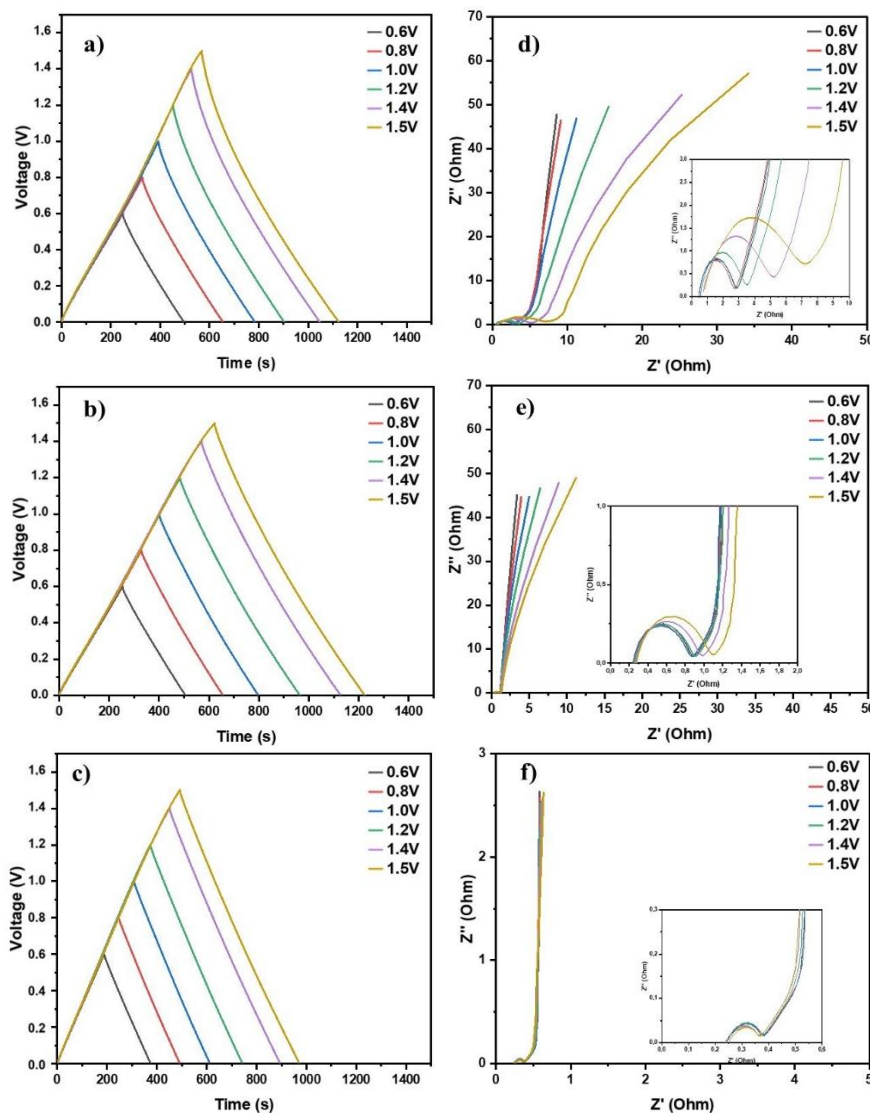


Figure 4. GCD (*a, b, c*), and EIS (*d, e, f*) of the RH-AC/KOH 2E cell at a current density of $0.2 \text{ A} \cdot \text{g}^{-1}$ with different voltages at 650, 750, and 850 °C, respectively

Figure 4(*b*) shows the GCD performance of RH-AC/KOH activated at 750 °C. The initial voltage drop during discharge is minimal and occurs within the time frame of 251 to 505 seconds. Additionally, the total discharge duration (ΔT) of 254 seconds suggests that the electrode materials have low internal resistance and excellent conductivity. Furthermore, the longest discharge time of 604 seconds is recorded at 1.5 V from 620 to 1224 seconds, directly reflecting the highest stored charge. Meanwhile, under comparable conditions, the GCD behavior of RH-AC/KOH activated at 750 °C with KOH remains notably higher than that of the RH-AC/KOH sample activated at 650 °C. Furthermore, at elevated voltages (1.4 V and 1.5 V), the charge-discharge curves exhibit a linear profile, maintaining symmetry between the charge and discharge lines. Figure 4(*e*) presents the Nyquist plot for RH-AC/KOH at 750 °C. At low voltages (0.6–1.2 V), the charge transfer resistance (R_{ct}) and equivalent series resistance (R_s) are similar, with values of 0.89 Ω and 0.26 Ω , respectively. As the voltage increases to 1.4 V and 1.5 V, the R_{ct} values rise slightly to 0.98 Ω and 1.1 Ω , respectively, forming a semicircle with a small radius, indicating that the electrochemical impedance of electrodes does not increase significantly. Meanwhile, the R_s values remain constant at 0.26 Ω throughout the tested voltage range of 0.6–1.5 V. Additionally, the conduction resistance exhibits minimal variation, ranging from 0.89 Ω to 1.1 Ω across the entire voltage range, consistently forming a distinct semicircle. Notably, the maximum change in charge transfer resistance (ΔR_{ct}) is only 0.21 Ω , which further confirms the stability of the system.

As can be seen in Figure 4(c), the initial voltage drop during discharge is minimal and occurs between 188.4 and 490 seconds. Moreover, the total discharge duration (ΔT) of 301.6 seconds indicates low internal resistance and excellent conductivity of the electrode materials. Notably, the longest discharge time is observed at 1.5 V, extending from 490 to 974 seconds. This maximum discharge duration (ΔT) of 484 seconds is directly proportional to the highest charge storage capacity. Furthermore, at higher voltages (1.4 V and 1.5 V), the charge-discharge curves exhibit a linear profile, maintaining symmetry between the charge and discharge lines. Figure 4(f) shows the RH-AC/KOH Nyquist plot at 850 °C. As the voltage increases to 0.6 V and 1.5 V, the equivalent series resistance (R_s) and charge transfer resistance (R_{ct}) values become similar at all six voltages. They increase slightly to 0.24 Ω and 0.38 Ω , respectively, indicating that the electrochemical resistance of the electrodes is very low and forming a semicircle with a very small radius. It is worth noting that the maximum change in charge transfer resistance (ΔR_{ct}) is only 0.14 Ω , confirming that the conductivity of the system is very low.

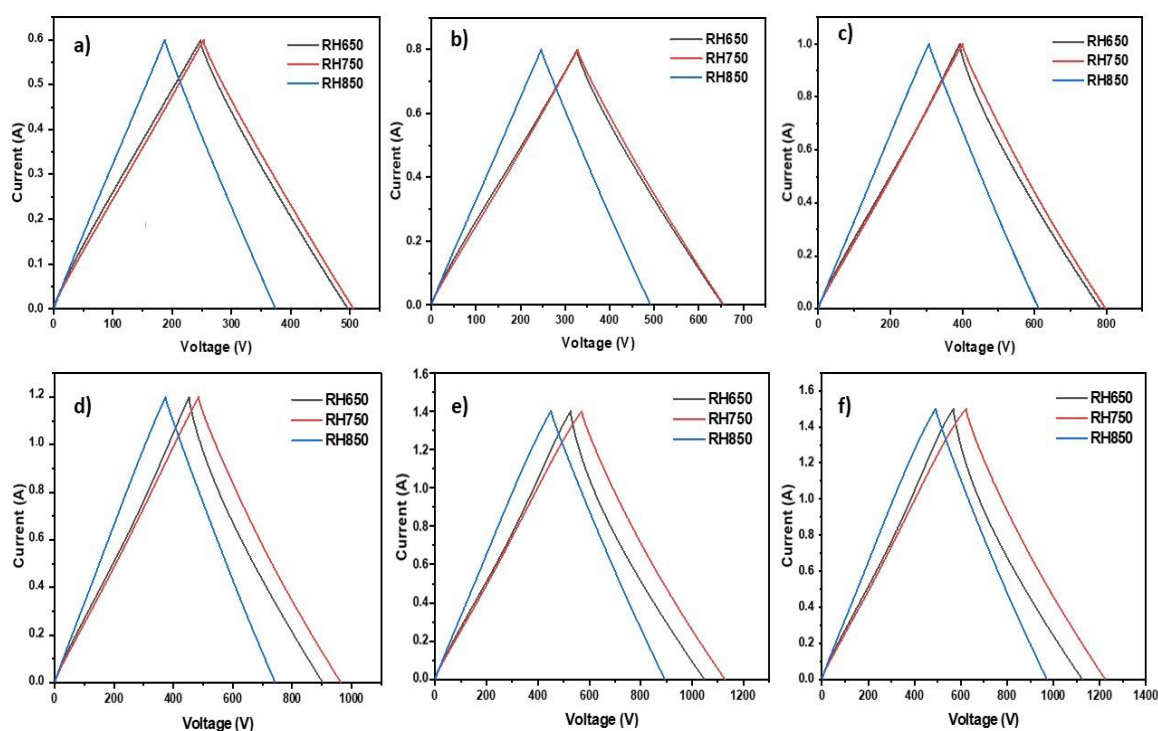


Figure 5. GCD versus 2E cell with RH-AC treated at 650, 750, and 850 °C at a current density of 0.2 A·g⁻¹ versus voltage: (a) 0.6 V, (b) 0.8 V, (c) 1.0 V, (d) 1.2 V, (e) 1.4 V, and (f) 1.5 V

Figure 5 demonstrates the galvanostatic charge-discharge behavior of a 2E cell containing RH-AC treated at 650 °C, 750 °C, and 850 °C at a current density of 0.2 A·g⁻¹ and over a wide range of voltage. Figure 5(a, b and c) shows the charge-discharge voltage variations for the RH/KOH sample treated at 850 °C (blue line) at voltages of 0.6 V, 0.8 V, and 1.0 V, which were 189 V, 246 V, and 306 V, respectively. These values indicate significantly lower capacitance than the other two samples, which were treated at 650 °C and 750 °C. Within the lower voltage range (0.6–1.0 V), the discharge voltage change values (ΔV) for the RH-650 °C and RH-750 °C samples remained consistent across figures a, b, and c. Furthermore, the ΔV values increased in the following order: 247 V < 326 V < 391 V for RH-650 °C and 253 V < 326 V < 400 V for RH-750 °C, respectively. On the other hand, when analyzing the graphs in Figure 5 (d, e, and f), it is evident that at relatively high voltages (1.2 V, 1.4 V, and 1.5 V), the charge-discharge curves are more widely spaced. Specifically, the discharge voltage changes (ΔV) increased in the order of 372 V < 444 V < 525 V for RH-850 °C, 451 V < 520 V < 556 V for RH-650 °C, and 481 V < 558 V < 607 V for RH-750 °C. These results indicate that the ΔV values for RH-850 °C were the lowest across all voltage tests, and the charge-discharge intersection angle formed an acute angle. Meanwhile, the discharge voltage changes (ΔV) for RH-650 °C and RH-750 °C followed a similar increasing trend. Additionally, as the voltage increased from 1.2 V to 1.5 V, the charge-discharge curves for RH-650 °C (brown line) became more arc-shaped, while the discharge voltage gradually decreased. In contrast, the RH-750 °C (red line) displayed the largest discharge

voltage change (ΔV) of $481 \text{ V} < 558 \text{ V} < 607 \text{ V}$, forming larger, symmetrical triangles and maintaining a steady increase.

Figure 6 illustrates the pronounced impact of activation temperature on the pore structure of RH-AC/KOH electrodes. At $650 \text{ }^\circ\text{C}$ (Fig. 6(a)), the RH-AC electrode exhibits a predominantly microporous structure, with micropores ($0.35\text{--}2 \text{ nm}$) accounting for 62.01% of the total porosity, along with a notable fraction of small mesopores ($2\text{--}10 \text{ nm}$) comprising 34.57% . Figure 6(b) shows that increasing the activation temperature to $750 \text{ }^\circ\text{C}$ leads to a clear shift in pore distribution: microporosity decreases to 52.69% , while mesoporosity increases to 40.58% . This trend reflects progressive pore widening, which is attributed to more intense KOH activation at higher temperatures. Furthermore, at $850 \text{ }^\circ\text{C}$ (Fig. 6(c)), the RH-AC/KOH electrode undergoes a dramatic structural transformation, with mesopores dominating at 89.98% and micropores nearly disappearing to 0.04% . This suggests that excessive activation at this temperature may lead to overdevelopment of mesopores and potential pore collapse. These results demonstrate the temperature-dependent tunability of the pore network, whereby elevated temperatures promote the formation of mesopores that enhance ion transport. However, this enhancement may come at the expense of a reduced specific surface area. This highlights the importance of optimizing activation conditions to achieve a balanced pore structure for optimal electrochemical performance.

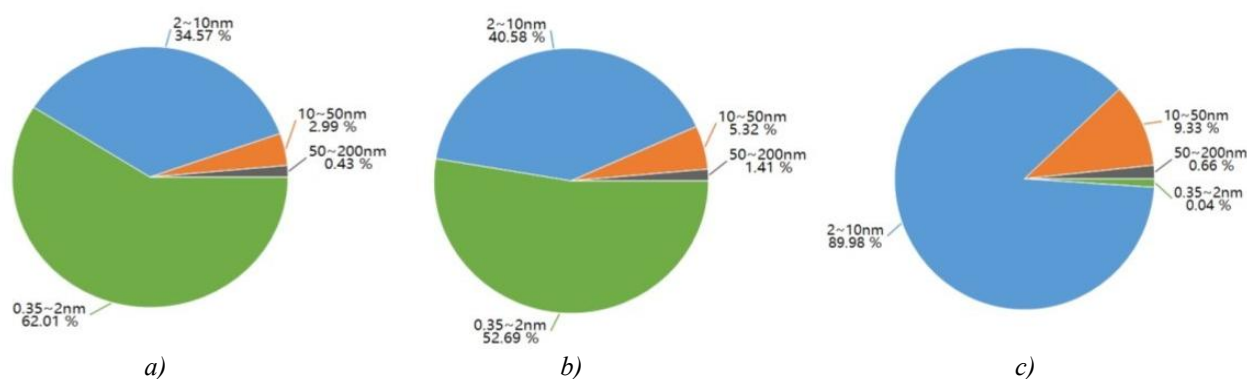


Figure 6. Pore volume distribution maps for RH-AC/KOH at 650 (a), 750 (b), and $850 \text{ }^\circ\text{C}$ (c) activated electrodes

This analysis confirms that the RH- $750 \text{ }^\circ\text{C}$ sample exhibits stable and high capacitance across a broad voltage range. Notably, it maintains superior performance at a current density of $0.2 \text{ A}\cdot\text{g}^{-1}$ under voltages higher than 1.5 V , demonstrating superior desirable characteristics for energy storage applications in supercapacitors.

Conclusions

Cyclic voltammetry (CV) tests reveal the electrochemical behavior of activated carbon samples, with RH-AC/KOH synthesized at $750 \text{ }^\circ\text{C}$ demonstrating the highest capacitance retention ($159\text{--}165 \text{ F}\cdot\text{g}^{-1}$). This superior performance is likely due to its optimized microporosity and enhanced conductivity, making it the most effective cathode material for supercapacitors. Electrochemical analysis, including galvanostatic charge-discharge (GCD) and electrochemical impedance spectroscopy (EIS), further confirms that RH-AC/KOH at $750 \text{ }^\circ\text{C}$ achieves the highest current density and maintains stable performance across a voltage range of $0.6\text{--}1.5 \text{ V}$, exhibiting the longest discharge duration. Comparing the specific current change (ΔSc) at low potentials ($0.6\text{--}1.0 \text{ V}$) among four samples of AC/NaOH at $850 \text{ }^\circ\text{C}$ and RH-AC/KOH at $650 \text{ }^\circ\text{C}$, $750 \text{ }^\circ\text{C}$ and $850 \text{ }^\circ\text{C}$ reveals the following trend: $281.2 > 269.2 > 267.6 > 190.5 \text{ mA}\cdot\text{g}^{-1}$. At higher potentials ($1.2\text{--}1.5 \text{ V}$), the ΔSc values follow the order: $341.9 \approx 340.0 > 314.6 > 247.8 \text{ mA}\cdot\text{g}^{-1}$. These results indicate that the AC/NaOH sample at $850 \text{ }^\circ\text{C}$ possesses the highest electrode density. However, the RH-AC/KOH sample treated at $750 \text{ }^\circ\text{C}$ exhibits the highest current density, compared the other RH-AC samples modified at different temperatures. Overall, the electrochemical data highlight the RH-AC/KOH sample treated at $750 \text{ }^\circ\text{C}$ as the most efficient electrode material. It delivers stable, high capacitance across different voltage levels and maintains superior performance at a current density of $0.2 \text{ A}\cdot\text{g}^{-1}$ above 1.5 V . The excellent electrochemical properties of rice husk-derived activated carbon synthesized at $750 \text{ }^\circ\text{C}$ underscore its strong potential as an advanced electrode material for supercapacitor energy storage. Its optimized porosity, improved electrical conductivity, and superior charge retention ensure high capacitance stability

over a broad voltage range. These attributes not only enhance energy storage efficiency but also indicate long-term durability and performance reliability, making it a promising candidate for next-generation supercapacitor applications in sustainable energy systems.

Funding

This research was funded by the Committee of Science of the Ministry of Science and Higher Education of the Republic of Kazakhstan (Grant No. BR27198045).

*Author Information**

*The authors' names are presented in the following order: First Name, Middle Name and Last Name

Nurbatyr Mukhametgazy — PhD, Satbayev University, 22a Satpaev str., 050013, Almaty, Kazakhstan; e-mail: nurbatyr.kaz@gmail.com; <https://orcid.org/0000-0001-5957-0305>

Kamila Maksatovna Temirkulova — 2nd year Master's Student, al-Farabi Kazakh National University, 71 Al-Farabi Ave., 050040; Satbayev University, 22a Satpaev str., 050013, Almaty, Kazakhstan; e-mail: t.kamila.m@mail.ru; <https://orcid.org/0009-0008-7238-0432>

Balauza Balgabayeva — 1st year Master's Student, al-Farabi Kazakh National University, 71 Al-Farabi Ave., 050040; Satbayev University, 22a Satpaev str., 050013, Almaty, Kazakhstan; e-mail: balaussa.balgabayeva002@gmail.com

Bekzat Gadylyly Khamzin — 1st year Master's Student, al-Farabi Kazakh National University, 050040, 71 Al-Farabi Ave.; Satbayev University, 22a Satpaev str., 050013, Almaty, Kazakhstan; e-mail: bekzatkhamzin@gmail.com; <https://orcid.org/0009-0003-7216-6552>

Seitkhan Azat — PhD, Associate Professor, Satbayev University, 22a Satpaev str., 050013, Almaty, Kazakhstan; e-mail: seytkhan.azat@gmail.com; <https://orcid.org/0000-0002-9705-7438>

Zhazira Asilbekovna Supiyeva (*corresponding author*) — PhD, Acting Associate Professor, al-Farabi Kazakh National University, 71 Al-Farabi Ave., 050040; Satbayev University, 22a Satpaev str., 050013, Almaty, Kazakhstan; e-mail: Zhazira.Supiyeva@kaznu.edu.kz; <https://orcid.org/0000-0002-5221-8605>

Qamar Abbas — Associate Professor, Poznan University of Technology, Poznan 60965, Poland; Graz University of Technology, Stremayrgasse 9, 8010 Graz, Austria; e-mail: qamar.abbas@put.poznan.pl; <https://orcid.org/0000-0002-1169-1906>

Author Contributions

The manuscript was written through contributions of all authors. All authors have given approval to the final version of the manuscript. **CRedit**: **Nurbatyr Mukhametgazy** investigation, formal analysis, visualization, writing-original draft; **Kamila Maksatovna Temirkulova** investigation, formal analysis, visualization; **Balauza Balgabayeva** resources, data curation, validation; **Bekzat Gadylyly Khamzin** formal analysis, visualization; **Seitkhan Azat** resources, funding acquisition, validation; **Zhazira Asilbekovna Supiyeva** funding acquisition, project administration, supervision, methodology, validation, writing-review & editing; **Qamar Abbas** conceptualization, methodology, writing-review & editing.

Acknowledgments

Authors gratefully acknowledge Satbayev University for providing access to library and research facilities that supported the completion of this work.

Conflicts of Interest

The authors declare no conflict of interest.

References

- Hassan, M.F., Sabri, M.A., Fazal, H., Hafeez, A., Shezad, N., & Hussain, M. (2020). Recent trends in activated carbon fibers production from various precursors and applications — A comparative review. *Journal of Analytical and Applied Pyrolysis*, 145, 104715. <https://doi.org/10.1016/j.jaap.2019.104715>

- 2 Pantrangi, M., Sambasivam, S., & Ran, F. (2022). Recent progress on biomass waste derived activated carbon electrode materials for supercapacitors applications — A review. *Journal of Energy Storage*, 54, 105290. <https://doi.org/10.1016/j.est.2022.105290>
- 3 Sevilla, M., & Mokaya, R. (2014). Energy storage applications of activated carbons: supercapacitors and hydrogen storage. *Energy Environ. Sci.*, 7(4), 1250–1280. <https://doi.org/10.1039/c3ee43525c>
- 4 De, S., Acharya, S., Sahoo, S., & Chandra Nayak, G. (2020). Present status of biomass-derived carbon-based composites for supercapacitor application. *Nanostructured, Functional, and Flexible Materials for Energy Conversion and Storage Systems*, 373–415. <https://doi.org/10.1016/b978-0-12-819552-9.00012-9>
- 5 Pavlenko, V.V., Abbas, Q., Przygocki, P., Kon'kova, T., Supiyeva, Z., Abeykoon, N., Prikhodko, N., Bijsenbayev, Kurbatov, M. A., Lesbayev, B.T., & Mansurov, Z.A. (2018). Temperature dependent characteristics of activated carbons from walnut shells for improved supercapacitor performance. *Eurasian Chemico-Technological Journal*, 20(2), 99–105. <https://doi.org/10.18321/ectj695>
- 6 Yerdauletov, M.S., Nazarov, K., Mukhametuly, B., Yeleuov, M.A., Daulbayev, C., Abdulkarimova, R., Yskakov, A., Napol'skiy, F., & Krivchenko, V. (2023). Characterization of Activated Carbon from Rice Husk for Enhanced Energy Storage Devices. *Molecules*, 28, 5818. <https://doi.org/10.3390/molecules28155818>
- 7 Supiyeva, Zh., Pan, X., & Abbas, Q. (2023). The critical role of nanostructured carbon pores in supercapacitors. *Current Opinion in Electrochemistry*, 39, 101249. <https://doi.org/10.1016/j.coelec.2023.101249>
- 8 Mensah-Darkwa, K., Agyemang, F.O., Akromah, S., Arthur, E. K., Abdallah, F., & Gikunoo, E. (2021). A comparative study on the performance of activated carbon electrodes and activated carbon/titanium dioxide nanotubes hybrid electrodes. *Scientific African*, 12, e00786. <https://doi.org/10.1016/j.sciaf.2021.e00786>
- 9 Reza, M.S., Yun, Ch.S., Afroze, Sh., Radenahmad, N., Abu Bakar, M.S., Saidur, R., Taweekun, J. & Azad, A.K. (2020). Preparation of activated carbon from biomass and its' applications in water and gas purification, a review. *Arab Journal of Basic and Applied Sciences*, 27:1, 208–238. <https://doi.org/10.1080/25765299.2020.1766799>
- 10 Gu, W., & Yushin, G. (2014). Review of nanostructured carbon materials for electrochemical capacitor applications: advantages and limitations of activated carbon, carbide-derived carbon, zeolite-templated carbon, carbon aerogels, carbon nanotubes, onion-like carbon, and graphene. *Wiley Interdisciplinary Reviews: Energy and Environment*, 3(5), 424–473. <https://doi.org/10.1002/wene.102>
- 11 Ntone, E.P.N., Samah, R.A., Wahab, M.S.A., Alsahy, Q.F. & Rahman, S.A. (2025). Review of PPCPs remediation in Asia: the role of agricultural waste in adsorption-membrane hybrid technology. *Chemical Engineering Communications*, 1–35. <https://doi.org/10.1080/00986445.2024.2447843>
- 12 Wu, F.C., Tseng, R.L., Hu, C.C., & Wang, C.C. (2005). Effects of pore structure and electrolyte on the capacitive characteristics of steam-and KOH-activated carbons for supercapacitors. *Journal of Power Sources*, 144(1), 302–309. <https://doi.org/10.1016/j.jpowsour.2004.12.020>
- 13 Liu, P., Verbrugge, M., & Soukiazian, S. (2006). Influence of temperature and electrolyte on the performance of activated-carbon supercapacitors. *Journal of Power Sources*, 156(2), 712–718. <https://doi.org/10.1016/j.jpowsour.2005.05.055>
- 14 Jackel, N., Weingarh, D., Schreiber, A., Krüner, B., Zeiger, M., Tolosa, A., Aslan, M. & Presser, V. (2016). Performance evaluation of conductive additives for activated carbon supercapacitors in organic electrolyte. *Electrochimica Acta*, 191, 284–298. <https://doi.org/10.1016/j.electacta.2016.01.065>
- 15 Du, X., Zhao, W., Wang, Y., Wang, C., Chen, M., Qi, T., etc. & Ma, M. (2013). Preparation of activated carbon hollow fibers from ramie at low temperature for electric double-layer capacitor applications. *Bioresour. Technol.*, 149, 31–37. <https://doi.org/10.1016/j.biortech.2013.09.026>
- 16 Tseng, R.L., Tseng, S.K., Wu, F.C., Hu, C.C., & Wang, C.C. (2013). Effects of micropore development on the physicochemical properties of KOH-activated carbons. *Journal of the Chinese Institute of Chemical Engineers*, 39(1), 37–47. <https://doi.org/10.1016/j.jcice.2007.11.005>
- 17 Lee, Kuan-Ching and Lim, Mitchell and Hong, Zhong-Yun and Chong, Siewhui and Tiong, Joyce and Pan, Guan-Ting and Huang, Chao-Ming (2021). Coconut Shell-Derived Activated Carbon for High-Performance Solid-State Supercapacitors. *Energies*, 14(15), 45–46. <https://doi.org/10.3390/en14154546>
- 18 Ranjeet Kumar Mishra, Bineta Singh, Bishnu Acharya (2024). A comprehensive review on activated carbon from pyrolysis of lignocellulosic biomass: An application for energy and the environment. *Carbon Resources Conversion*, 7(4). 100228. <https://doi.org/10.1016/j.crcon.2024.100228>
- 19 Yang, Juan & Qiu, Keqiang. (2010). Preparation of Activated Carbons from Walnut Shells via Vacuum Chemical Activation and Their Application for Methylene Blue Removal. *Chemical Engineering Journal*, 165, 209–217. <https://doi.org/10.1016/j.cej.2010.09.019>
- 20 Harshal Kulkarni, Chandresh Bari, Sagnik Mukherjee, Prayag Gajera, Govind Sethia (2024). Waste biomass-derived activated carbons for selective oxygen adsorption. *Carbon Trends*, 17, 100398. <https://doi.org/10.1016/j.cartre.2024.100398>
- 21 Smagulova, G., Imash, A., Baltabay, A., Kaidar, B., & Mansurov, Z. (2022). Rice-Husk-Based Materials for Biotechnological and Medical Applications. *MDPI Carbons*, 8(4), 55. <https://doi.org/10.3390/c8040055>
- 22 Azat, S., Korobeinyk, A.V., Moustakas, K., & Inglezakis, V.J. (2019). Sustainable production of pure silica from rice husk waste in Kazakhstan. *Journal of Cleaner Production*, 217, 352–359. <https://doi.org/10.1016/j.jclepro.2019.01.142>
- 23 Kurmanbayeva, I., Mentbayeva, A., Sadykova, A., Adi, A., Mansurov, Z., & Bakenov, Z. (2019). Silica from Kazakhstan Rice Husk as an Anode Material for LIBs. *Eurasian Chemico-Technological Journal*, 1, 75. <https://doi.org/10.18321/ectj794>

- 24 Mansurov, Z.A., Smagulova, G.T., Sultanov, F.R., Kaidar, B.B., Insepov, Z., & Imash, A.A. (2022). Production of activated and Graphene-Like Carbon Materials from rice husk. *Materials Science*, 2210–08352. <https://doi.org/10.48550/arXiv.2210.08352>
- 25 Battalova, A., Ibraeva, Z., Kabdrakhmanova, S., Akatan, K., Shaimardan, E., Demeukhan, A., Tursyngazykyzy, A., Beisebekov, M., & Maussumbayeva, A. (2024). Comparative characteristics of microcrystalline cellulose obtained from the rice waste production of Kazakhstan. *Chemical Bulletin of Kazakh National University*, 113(4), 14–23. <https://doi.org/10.15328/cb1386>
- 26 Zhu, G., Deng, X., Hou, M., Sun, K., Zhang, Y., Li, P., & Liang, F. (2016). Comparative study on characterization and adsorption properties of activated carbons by phosphoric acid activation from corncob and its acid and alkaline hydrolysis residues. *Fuel Processing Technology*, 144, 255–261. <https://doi.org/10.1016/j.fuproc.2016.01.007>
- 27 Kierzek, K., & Gryglewicz, G. (2020). Activated carbons and their evaluation in electric double layer capacitors. *Molecules*, 25(18), 4255. <https://doi.org/10.3390/molecules25184255>
- 28 Song H, Qu Q, Yang Z, Zhang Y, Qiu L, Zhao Y, Li C, Zhu M, & Yang X. (2025). Supercapacitor Performance of Activated Carbon from *Eucommia Ulmoides* Oliver Wood Optimized by the Activation Method. *ACS Omega*, 10(15), 15368–15380. <https://doi.org/10.1021/acsomega.4c11529>
- 29 Bergna, D., Hu, T., Prokkola, H. Prokkola, H., Romar, H., & Lassi, U. (2020). Effect of Some Process Parameters on the Main Properties of Activated Carbon Produced from Peat in a Lab-Scale Process. *Waste Biomass Valor*, 11, 2837–2848. <https://doi.org/10.1007/s12649-019-00584-2>
- 30 Foo, K.Y., & Hameed, B.H. (2012). Preparation and characterization of activated carbon from pistachio nut shells by microwave-induced chemical activation: Application for methylene blue adsorption. *Chemical Engineering Journal*, 180, 66–74. <https://doi.org/10.1016/j.cej.2011.11.044>
- 31 Nahil, M.A., & Williams, P.T. (2012). Characterisation of Activated Carbons with High Surface Area and Variable Porosity Produced from Agricultural Cotton Waste by Chemical Activation and Co-activation. *Waste Biomass Valor* 3, 117–130. <https://doi.org/10.1007/s12649-012-9109-7>
- 32 Jiang, Q., Zhang, Q., Du, B., Zou, R.L., Liu, Y.H., & Zhao, Y. (2008). Effects of activation time on the electrochemical capacitance of activated carbon nanotubes. *Journal of Materials Science: Materials in Electronics*, 19, 241–245. <https://doi.org/10.1007/s10854-007-9291-8>
- 33 Wang, D.W., Li, F., Liu, M., Lu, G. Q., & Cheng, H.M. (2008). 3D aperiodic hierarchical porous graphitic carbon material for high-rate electrochemical capacitive energy storage. *Angewandte Chemie International Edition*, 47(2), 373–376. <https://doi.org/10.1002/anie.200704528>
- 34 Wang, J., & Kaskel, S. (2012). KOH activation of carbon-based materials for energy storage. *Journal of Materials Chemistry*, 22(45), 23710–23725. <https://doi.org/10.1039/c2jm34066f>
- 35 Supiyeva, Zh., Avchukir, Kh., Pavlenko, V., Yeleuov, M., Taurbekov, A., Smagulova, G., & Mansurov, Z. (2020). The investigation of electroreduction of AuCl₄ in the case of gold electroreduction using activated carbon. *Materials Today: Proceedings*, S2214785319336958. <https://doi.org/10.1016/j.matpr.2019.11.013>
- 36 Pavlenko, V., & Supiyeva, Z. (2020). Application of Carbons Produced from Rice Husk in the Process of Capacitive Deionization. *Eurasian Chemico-Technological Journal*, 22(4), 277–284. <https://doi.org/10.18321/ectj996>
- 37 Taurbekov, A., Abdisattar, A., Atamanov, M., Yeleuov, M., Daulbayev, C., Askaruly, K., Kaidar, B., Mansurov, Z., Castro-Gutierrez, J., Celzard, A., et al. (2023). Biomass Derived High Porous Carbon via CO₂ Activation for Supercapacitor Electrodes. *Journal of Composites Science*, 7(10), 444. <https://doi.org/10.3390/jcs7100444>
- 38 Zhang, Z.J., Xie, D.H., Cui, P., & Chen, X.Y. (2014). Conversion of a zinc salicylate complex into porous carbons through a template carbonization process as a superior electrode material for supercapacitors. *RSC advances*, 4(13), 6664–6671. <https://doi.org/10.1039/C3RA44981E>